Manipulating Core Excitations in Molecules by X-Ray Cavities

Bing Gu,[1,*] Artur Nenov,[2,*] Francesco Segatta,[2] Marco Garavelli,[2,†] and Shaul Mukamel[1,‡]
[1]Department of Chemistry and Department of Physics and Astronomy, University of California, Irvine, California 92697, USA
[2]Dipartimento di Chimica Industriale "Toso Montanari," Università degli studi di Bologna, Viale del Risorgimento 4, 40136 Bologna, Italy

(Received 27 August 2020; revised 2 December 2020; accepted 22 December 2020; published 4 February 2021)

Core excitations on different atoms are highly localized and therefore decoupled. By placing molecules in an x-ray cavity the core transitions become coupled via the exchange of cavity photons and form delocalized hybrid light-matter excitations known as core polaritons. We demonstrate these effects for the two inequivalent carbon atoms in 1,1-difluoroethylene. Polariton signatures in the x-ray absorption, two-photon absorption, and multidimensional four-wave mixing signals are predicted.

DOI: 10.1103/PhysRevLett.126.053201

Hybrid light-matter states between the material polarization and cavity photon modes, known as polaritons, are created when the light-matter coupling strength is larger than the decay rate of the cavity mode and the decoherence rate of the molecular transition (the strong coupling regime). When the cavity mode is in the vacuum state, the effective coupling strength for an assembly of N identical molecules is $\kappa = g\sqrt{N}\mu$, $g \equiv \sqrt{\hbar\omega_c/2\varepsilon_0 V_c}$, where ε_0 is the electric permittivity of vacuum, ω_c the cavity frequency, μ the transition dipole moment, and V_c is the cavity mode volume [1]. The $\sqrt{N}$ factor is responsible for cooperative superradiance [2,3]. Cavity polaritons in the visible and infrared regime have long been studied in atoms and were recently experimentally reported in molecules [4–11]. Molecular electronic and vibrational polaritons have been experimentally shown to alter the electronic, optical, and chemical properties of molecules including photoisomerization, electronic energy transfer, electron transfer, and ground-state reaction rates [9]. These findings triggered intensive theoretical investigations [3,6,12–30].

Thin-film optical cavities in the hard x-ray regime have been recently employed in the study of collective Mössbauer signals of ^{57}Fe nuclei (14.4 keV) [31–33] and tantalum L-edge x-ray spectra (9881 eV) [34]. A ~ 41 eV effective light-molecule coupling strength for low-finesse x-ray cavities has been reported [34]. X-ray cavities in the soft x-ray regime can be formed by alternating nanometer layers of materials with different indices of refraction, and are on the horizon. For high-reflectivity mirrors, the cavity photon modes satisfy $(n+\frac{1}{2})\lambda_n = L$, where L is the cavity length and λ_n is the wavelength of the cavity mode. For carbon K edge ($\sim$300 eV), it corresponds to $L \sim 10$ nm.

Here we study molecular polariton effects in the x-ray regime whereby a high-finesse x-ray cavity mode couples to molecular core excitations. We demonstrate that localized excitations from inequivalent carbon core orbitals in 1,1-difluoroethylene can be coupled by the exchange of an x-ray cavity photon, leading to hybrid core excitation with x-ray cavity photon modes. Rich exciton-polariton physics has been observed in the optical regime. This includes long-range transport [35,36], enhanced optical nonlinearity, modified chemical reactions, polariton lasers, optical transistors, and phase transitions [9]. Our study suggests that similar phenomena may be expected for core polaritons in the x-ray regime. X-ray cavities enable long-range transport of core excitons or core holes despite their highly localized nature as long as the light-matter coupling strength is stronger than their decay rates [35,36]. We predict signatures of core polaritons in the x-ray absorption spectrum, in two-dimensional (2D) x-ray four-wave mixing signals: photon echo (PE) and double quantum coherence (DQC), and in the two-photon absorption. Time-domain 2D spectroscopic techniques provide a versatile tool for exploring the optical properties of matter [37,38]. Multidimensional x-ray spectroscopy enabled by x-ray lasers [39] can [40–42] capture electron dynamics on the attosecond (as) timescale, and can reveal the correlations among core excitations.

We consider a system of N molecules coupled to a single x-ray cavity mode described by the Hamiltonian $H = H_{\rm M} + H_{\rm CM} + H_{\rm LM}(t) + H_{\rm C}$, where the nth molecular Hamiltonian $H_{\rm M}^{(n)} = \sum_{j\in\{g,e,f\}} \hbar\omega_j |j^{(n)}\rangle\langle j^{(n)}|$, the cavity Hamiltonian $H_{\rm C} = \hbar\omega_c a^\dagger a$, and the cavity-molecule coupling $H_{\rm CM} = \sum_{n=1}^{N} -\boldsymbol{\mu}^{(n)}\cdot\hat{\mathbf{E}}(\mathbf{r}_n,t)$. Here $\boldsymbol{\mu}^{(n)}$ is the transition dipole moment and $\hat{\mathbf{E}}(\mathbf{r}) = i\sqrt{\hbar\omega_c/2\varepsilon_0 V_c}\,\mathbf{e}_c a e^{i\mathbf{k}_c\cdot\mathbf{r}} +$ H.c. is the electric field operator where a ($a^\dagger$) is the boson annihilation (creation) operator for the cavity mode, $\mathbf{k}_c$, $\mathbf{e}_c$ are the cavity mode wave vector and polarization, respectively, H.c. stands for the Hermitian conjugate. We focus on the single- and double-core carbon K-edge excited states, labeled e and f, respectively. Double-core excitations of the same carbon atom are excluded, as they are blueshifted by

tens of eV with respect to doubly core-excited states on different atoms [43]. This shift can be attributed to the reduced electron shielding caused by the first core excitation which shifts a second core excitation from the same atom to the blue. The electric-dipole coupling $H_{\mathrm{LM}}(t)$ describes the interaction of the molecules with external laser pulses.

For $N > 1$ and $|\mathbf{k}_c \cdot (\mathbf{r}_n - \mathbf{r}_m)| \ll 1$, it is convenient to introduce the collective core-exciton states $|E_{\alpha k}\rangle = (1/\sqrt{N}) \sum_{n=1}^{N} e^{ikn} |g^{(1)} \cdots g^{(n-1)} e_\alpha^{(n)} g^{(n+1)} \cdots\rangle$ describing a superposition of a single excitation shared by all molecules and similarly $|F_{\mu k}\rangle$, where $k = 2\pi j/N$, $j = 0, \ldots, N-1$. Here α and μ run over the singly and doubly excited states, respectively. Up to double excitations, the cavity-molecule coupling can be represented by (see Sec. S1 in Supplemental Material for details [44])

$$H_{\mathrm{CM}} = \sum_{\alpha} \sqrt{N}\, \kappa_{e_\alpha g} |E_{\alpha 0}\rangle\langle G| a + \sum_{k} \sum_{\mu,\alpha} \kappa_{f_\mu e_\alpha} |F_{\mu k}\rangle\langle E_{\alpha k}| a + \sum_{n \neq m} \sum_{\alpha,\beta} \kappa_{e_\alpha g} |e_\alpha^{(n)} e_\beta^{(m)}\rangle\langle e_\beta^{(m)}| a + \mathrm{H.c.}, \quad (1)$$

where $|G\rangle = |g^{(1)} \cdots g^{(N)}\rangle$. Equation (1) implies that the transition from the ground state to the delocalized core-exciton states $|E_{\alpha 0}\rangle$ is enhanced by $\sqrt{N}$, whereas the coupling between excited states $|E_{\alpha k}\rangle$ and $|F_{\mu k}\rangle$ does not show such cooperativity [3]. The bright state $|E_{\alpha 0}\rangle$ is invariant under exchange of any two molecules. The dark states $|E_{\alpha k}\rangle$, $k \neq 0$ do not contribute to the absorption spectrum. Nevertheless, the transitions between the single-polariton and the dark biexciton states are coupled to the cavity mode by the $|F_{\mu k}\rangle\langle E_{\alpha k}| a + \mathrm{H.c.}$ term even for $k \neq 0$. Note that bright polariton states can relax to the dark states due to, e.g., vibronic couplings, disorder, and cavity loss [3,59]. The third term in Eq. (1) represents the coupling between the singly and doubly core-excited states from different molecules (Sec. S1 of Supplemental Material [44]).

Figure 1 depicts the ground-state structure of 1,1-difluoroethylene optimized at the Møller-Plesset second-order perturbation level, and compares the simulated and experimental x-ray absorption near edge structure (XANES) in the [280, 296] eV spectral range. This molecule has two inequivalent carbon atoms with bound preedge transitions separated by a few eV. The electronic structure computations are detailed in Sec. S2 and the spectroscopic simulations in Sec. S3 [44] The simulated XANES spectrum (without any shift) is in excellent agreement with experiment in the [280, 296] eV spectral range. The spectrum has four main features. The 285.6 and 289.5 eV peaks are associated with excitations from the $1s$ core orbitals of the carbon atoms in the CH_2 and CF_2 groups to the antibonding π^* orbital, respectively. A broader peak at 293 eV arises from a pair of close lying

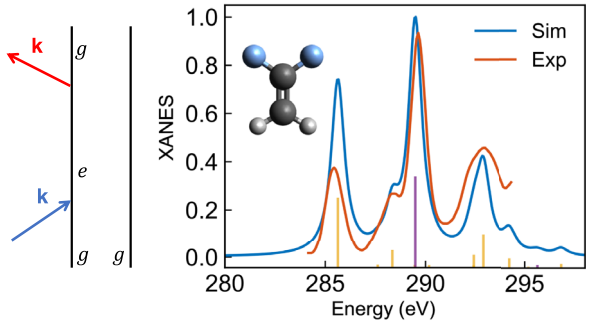

FIG. 1. The XANES spectrum of 1,1-difluoroethylene and the corresponding (left) Feynman diagram. $\mathbf{k}$ denotes the incoming pulse wave vector. Right: The transitions involving the carbon K-edge in CH_2 (CF_2) are represented by yellow (purple) sticks. The agreement with experiment [60] is excellent.

transitions from CH_2 to Rydberg (Ry) orbitals. Finally, we find a red shoulder to the 289.5 eV band at 288.4 eV, associated with a transition from CH_2 to a σ^* antibonding orbital localized in the CH_2 fragment. The ~4 eV energy splitting between the $CH_2 \to \pi^*$ and $CF_2 \to \pi^*$ peaks shows that functionalization with electron withdrawing groups such as fluorine makes core excitations more energy costly, thus inducing a few eV blueshift. The K-edge spectrum is dominated by the core excitations of CH_2.

In the x-ray cavity, the core excitations are modified by coupling to the cavity mode. Figure 2 (top) illustrates the XANES of core polaritons at cavity frequencies $\omega_c = 290$ eV close to the $CF_2 \to \pi^*$ excitation for varying coupling strength. At $g\sqrt{N} = 2.45$ eV/D, we observe a vacuum Rabi splitting of two polariton peaks. The transition dipole is in the order of 0.1 D. The Rabi splitting is increased with the coupling strength, and the lower polariton further mixes with CH_2 excitations leading to enhancement and redshift of the $CH_2 \to \pi^*$ transition.

To unveil the polaritonic nature of the core excitations in the x-ray cavity, we have decomposed each polariton state into the CH_2, CF_2, and the cavity photon components. These are depicted in the lower panels in Fig. 2. Since the core excitations localized at CH_2 and CF_2 are decoupled, each excitation is either purely CH_2 or CF_2 type. To decompose the polariton states, we introduce the projection operators $P_\sigma = \sum_{\alpha \in \sigma} |e_\alpha\rangle\langle e_\alpha|$, where $\sigma = \{\text{cavity photon}, \mathrm{CH_2}, \mathrm{CF_2}\}$. The σ component in a polariton state $|\Psi\rangle$ is computed as $\langle\Psi|P_\sigma|\Psi\rangle$. As shown in Fig. 2, without cavity ($g = 0$), all excitations are either purely CH_2 (yellow) or CF_2 (purple) type. As the coupling is turned on, the two ~290 eV excitations contain mixed CF_2 and photon (brown) character, reflecting a hybridization of the $CF_2 \to \pi^*$ and the cavity photon, resembling the polariton states in a Jaynes-Cummings model. As g increases, the polariton states further mix with CH_2 excitations, leading to delocalized core excitations from both CH_2 and CF_2. The delocalization can be

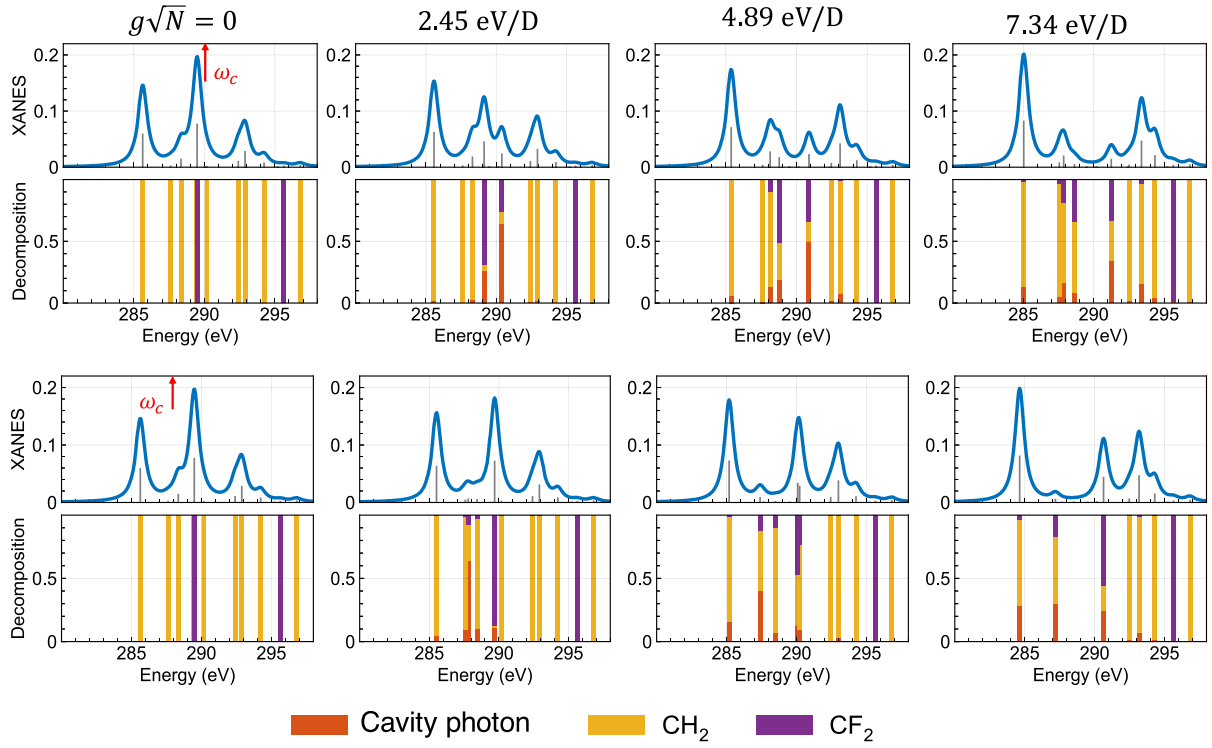

FIG. 2. XANES of 1,1-difluoroethylene in an x-ray cavity for varying coupling strength. Lower panels show the decomposition of each polariton state into CH_2, CF_2, and photon components. The top row is for cavity frequency $\omega_c = 290$ eV close to a specific transition, and the bottom row for cavity frequency $\omega_c = 288$ eV detuned from the main core transitions. The dependence on N is solely through the (collective) coupling strength $g\sqrt{N}$.

clearly observed in the decomposition of the polariton states ~290 eV. These delocalized excitations involving both C atoms arise from an effective coupling between their core excitations induced by exchanging cavity photons even when the cavity is in the vacuum state. When the cavity frequency is detuned far from any resonance in the bare XANES $\omega_c = 288$ eV (bottom row of Fig. 2), no substantial changes in the spectrum are observed at $g = 2.45$ eV/D. Nevertheless, as g gets stronger, we observe similar delocalized core excitations involving both CH_2 and CF_2 at, e.g., 290 eV.

For nonlinear x-ray signals, we focus on the single-molecule $N = 1$ strong coupling case. Single-molecule strong coupling requires a substantial field enhancement, and its realization may benefit from an ensemble of auxiliary emitters [61]. The signals for large N can depend on many collective dark states that are neglected here. Doubly core-excited dark states $|e_\alpha^{(n)} e_\beta^{(m)}\rangle$ in different molecules also need to be taken into account. Such states do not show up in bare nonlinear spectroscopy due to destructive interference [62,63]. The cavity mode mediates an effective coupling even for otherwise noninteracting molecules, and the two-core-exciton states from different molecules will influence the bipolariton manifold. Below, g, e, f label the ground, single-polariton, and two-polariton states, respectively; see Fig. 3 for the level scheme.

We have computed time-domain heterodyne-detected 2D x-ray four-wave mixing signals of core polaritons. These allow us to track the time evolution of the polariton states and reveal correlations between transitions. The total electric field is decomposed into three pulses, $E(t) = E_3(t) + E_2(t+T_2) + E_1(t+T_1+T_2) + \text{c.c.}$, where T_j is the time delay between the jth and $(j+1)$th pulse. Labeling the wave vectors of the incoming pulses as $\mathbf{k}_j$, we first discuss photon echo signal at $-\mathbf{k}_1 + \mathbf{k}_2 + \mathbf{k}_3$.

The 2D PE spectra are sketched by the Liouville space pathways represented by Feynman diagrams [37], depicted in Fig. S1 of Supplemental Material [44]. The 2D correlation spectra are obtained by Fourier transforming the delays T_1 (coherence time) and $T_3 \equiv t$ (detection time) in the polarization $S_{\text{PE}}(\Omega_3, \Omega_1; T_2) = \int_0^\infty dT_1 \int_0^\infty dT_3 \langle P_{\text{PE}}(T_3, T_2, T_1)\rangle e^{i\Omega_3 T_3 + i\Omega_1 T_1}$.

The 2D PE signals are displayed in Fig. 3. There are three contributions to the spectra: stimulated emission (SE) and ground-state bleaching (GSB) (the first two diagrams in Fig. S1 [44]) and the excited state absorption (ESA) (the last diagram in Fig. S1 [44]). The four XANES features discussed earlier give rise to four traces along Ω_1 (i.e., CH_2 excitations at 285.6, 288.4, and 293.0 eV and CF_2 excitations at 289.5 eV) with a characteristic cross peak pattern, that reflects the correlation between various transitions. The cross peaks result from the fact that they share a common

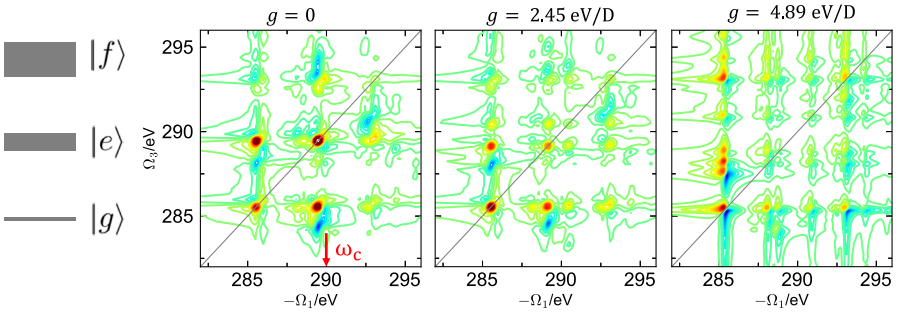

FIG. 3. Level scheme and the 2D photon echo spectra $S_{\mathrm{PE}}(\Omega_3, \Omega_1; T_2 = 0)$ for 1,1-difluoroethylene in an x-ray cavity with $\omega_c = 290$ eV for different coupling strengths as indicated. We use attosecond pulses with central frequency 290 and 20 eV bandwidth.

ground state, and that the core excitations are both anharmonic $\omega_{fe} \neq \omega_{eg}$ and coupled $\omega_{fg} \neq \omega_{eg} + \omega_{e'g}$. ESA signals related to double core excitations from the same carbon atom do not cancel the respective GSB and SE signals, consequently, cross peaks appear symmetrically below and above the diagonal. Transitions involving CH_2 and CF_2 cores are quartically coupled due to spatial vicinity of the two carbons; i.e., excitations of CH_2 core depends on the occupation number in CF_2 and vice versa. The associated ESA exhibit a $\sim$1.5 eV redshift $(\Omega_1, \Omega_3) = (289.6\ \mathrm{eV}, 284.0\ \mathrm{eV})$ and $(285.6\ \mathrm{eV}, 288.0\ \mathrm{eV})$ or a blueshift $(289.6\ \mathrm{eV}, 294.5\ \mathrm{eV})$ and $(293.0\ \mathrm{eV}, 291.0\ \mathrm{eV})$ with respect to the corresponding off-diagonal GSB which makes the ESA appear in the 2D spectra. At $g = 2.45$ eV/D, the polariton splitting is reflected in the additional cross peaks between the polariton states and bare molecular states. Similar features are seen in the stronger coupling case shown in Fig. 3 where additional hybrid polariton states containing excitations from both carbon atoms are created.

We now turn to the DQC signal at $\mathbf{k}_1 + \mathbf{k}_2 - \mathbf{k}_3$ [64–68], represented by the diagrams shown in Fig. S2 [44]. The correlations between single and two polaritons can be obtained either by Fourier transform of the time delays T_3 and T_2 at a fixed T_1, $S_{\mathrm{DQC}}(\Omega_3, \Omega_2; T_1)$ or by Fourier transform of the time delays T_1 and T_2 at a fixed T_3 $S_{\mathrm{DQC}}(\Omega_2, \Omega_1; T_3)$. In DQC, the polariton system is in the coherence $|e\rangle\langle g|$ during T_1, and is then promoted to $|f\rangle\langle g|$ during T_2. The system can be either $|f\rangle\langle e|$ or $|e\rangle\langle g|$ for the detection time T_3. The peaks in $S_{\mathrm{DQC}}(\Omega_2, \Omega_1; T_3)$ reveal correlation between ω_{eg} and ω_{fg}. For a harmonic system where $\omega_{fg} = \omega_{eg}$ and for uncorrelated transitions where $\omega_{fg} = \omega_{eg} + \omega_{e'g}$, the DQC signal vanishes as the two contributions to DQC interfere destructively. This makes DQC suitable for resolving anharmonicities and correlated transitions.

The DQC $S_{\mathrm{DQC}}(\Omega_2, \Omega_1; T_3)$ are shown in Fig. 4 for varying cavity coupling strengths. The vertical axis shows the doubly core-excited states $|f\rangle$ that can be reached from $|g\rangle$ through an excited state $|e\rangle$. Prominent contributions at $(\Omega_1, \Omega_2) = (285.6\ \mathrm{eV}, 573.9\ \mathrm{eV})$ and $(289.5\ \mathrm{eV}, 573.9\ \mathrm{eV})$ arise due to the coupling of $CH_2 \rightarrow \pi^*$ (285.6 eV) and $CF_2 \rightarrow \pi^*$ (289.5 eV) transitions to the CH_2, $CF_2 \Rightarrow \pi^*$ transition [69]. Similarly, peaks at $(289.5\ \mathrm{eV}, 584.1\ \mathrm{eV})$ and $(293.0\ \mathrm{eV}, 584.1\ \mathrm{eV})$ arise due to the coupling of $CF_2 \rightarrow \pi^*$ (289.5 eV) and $CH_2 \rightarrow$ Ry (293.0 eV) transitions to the CH_2, $CF_2 \Rightarrow \pi^*$, Ry transition. In the strong coupling regime, the polariton states manifest as a doublet around $\Omega_1 = 290$ eV. Additional peaks are clearly observed between these single-polariton states and the f manifold. Core polaritons also modulate the doubly core-excited states by mixing them with the two-cavity-photon state and single-core-excitation single-cavity-photon state. For example, a noticeable redshift can be observed for the CH_2, $CF_2 \Rightarrow \pi^*$ transition from the slices of the DQC at $\Omega_1 = 285.5$ eV.

The correlations between ω_{fe} and ω_{fg} are revealed in the DQC signal $S_{\mathrm{DQC}}(\Omega_3, \Omega_2; T_1)$ displayed in Fig. 4 (bottom

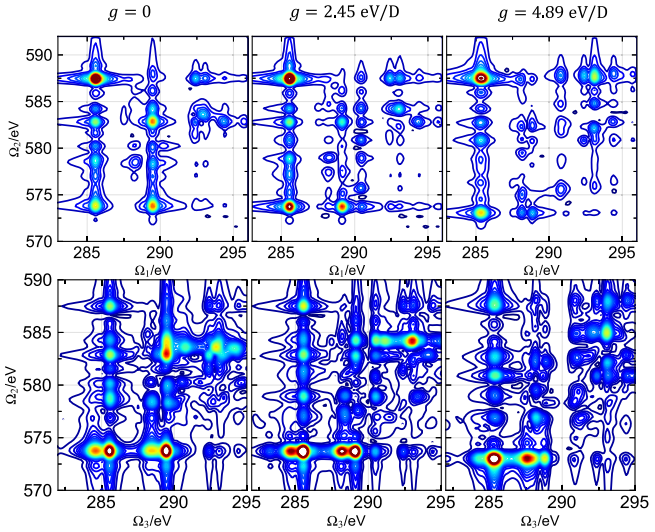

FIG. 4. 2D double quantum coherence spectra $|S_{\mathrm{DQC}}(\Omega_2, \Omega_1; T_3)|$ (upper row) and $|S_{\mathrm{DQC}}(\Omega_3, \Omega_2; T_1)|$ (lower row) in an x-ray cavity with $\omega_c = 290$ eV at different coupling strengths g as indicated. A small time delay 10^{-5} as is used for both T_3 and T_1 to avoid cancellation of the two DQC diagrams.

row). States from the doubly excited manifold coupled to the singly excited manifold are characterized through a set of four peaks along Ω_3 for a given Ω_2 value [70]. For example, the quartet of peaks along the $\Omega_2 = 573.9$ eV are associated with two peaks at 285.6 eV and 289.5 eV coinciding with the $CH_2 \rightarrow \pi^*$ and $CF_2 \rightarrow \pi^*$ transitions and two red-shifted peaks at 284.4 and 288.3 eV corresponding to the $CH_2 \rightarrow \pi^*$ with CF_2 excited and $CF_2 \rightarrow \pi^*$ with CH_2 excited [71]. The 1.2 eV splitting corresponds to the value of the quartic coupling between both transitions. Under strong coupling, core-polariton doublets can be observed along Ω_3 due to the ω_{fe} resonances. The splitting does not directly correspond to the polariton resonances because both e and f manifolds are modified by the cavity mode.

Similar information about the correlations of single and double excitations as provided by DQC can be extracted from the two-photon absorption signal, discussed in Sec. S4 of Supplemental Material [44]. This signal does not require coherent x-ray pulses and is thus easier to implement experimentally.

In summary, we have demonstrated how molecular core excitations can be manipulated by coupling to the vacuum field in an x-ray cavity. Localized excitations from the two carbon atoms in 1,1-difluoroethylene are coherently coupled by the exchange of an x-ray cavity photon creating hybrid delocalized excitations. We identified the spectroscopic signatures of core polaritons in XANES, two-photon absorption, and multidimensional x-ray spectroscopic signals. XANES directly probes the hybrid core-polariton states with the polariton effects manifested as mode splitting, redistribution of oscillator strength, and line shifts, depending on the cavity frequency and coupling strength. Correlations between polaritonic excitations are revealed by the PE, and information about the two-polariton manifold can be readily extracted from the DQC and two-photon absorption signals. This study shows how to manipulate core excitations in molecules by strong coupling to a cavity in the x-ray regime. Many interesting phenomena discovered for exciton polaritons in the optical regime such as long-range transport [35], modified chemical reaction rates [72], and enhanced nonlinearity [36] suggest analogous extensions for core polaritons in the x-ray regime. Relaxation dynamics of core polaritons is also expected to differ significantly from the bare core excitations. Collective effects found in Mössbauer resonance in iron including electromagnetically induced transparency and Lamb shift [32,33] may show up in molecules as well.

We thank Dr. Stefano M. Cavaletto for helpful discussions and Dr. Ralf Röhlsberger for valuable feedback. M. G., A. N., F. S., and S. M. acknowledge support from the Chemical Sciences, Geosciences, and Bio-sciences division, Office of Basic Energy Sciences, Office of Science, U.S. Department of Energy, through Award No. DE-SC0019484. B. G. acknowledges the support from the National Science Foundation Grant No. CHE-1953045.

*These authors contributed equally to this work.
†marco.garavelli@unibo.it
‡smukamel@uci.edu

[1] E. M. Purcell, Spontaneous emission probabilities at radio frequencies, Phys. Rev. **69**, 681 (1946), http://pages.erau.edu/~reynodb2/colloquia/Purcell_1946_SpontaneousEmission.pdf.
[2] R. H. Dicke, Coherence in spontaneous radiation processes, Phys. Rev. **93**, 99 (1954).
[3] M. Kowalewski, K. Bennett, and S. Mukamel, Femtochemistry: Manipulating nonadiabatic dynamics at avoided crossings, J. Phys. Chem. Lett. **7**, 2050 (2016).
[4] X. Zhong, T. Chervy, L. Zhang, A. Thomas, J. George, C. Genet, J. A. Hutchison, and T. W. Ebbesen, Energy transfer between spatially separated entangled molecules, Angew. Chem., Int. Ed. Engl. **56**, 9034 (2017).
[5] J. George, A. Shalabney, J. A. Hutchison, C. Genet, and T. W. Ebbesen, Liquid-phase vibrational strong coupling, J. Phys. Chem. Lett. **6**, 1027 (2015).
[6] A. Shalabney, J. George, J. Hutchison, G. Pupillo, C. Genet, and T. W. Ebbesen, Coherent coupling of molecular resonators with a microcavity mode, Nat. Commun. **6**, 5981 (2015).
[7] F. Benz, M. K. Schmidt, A. Dreismann, R. Chikkaraddy, Y. Zhang, A. Demetriadou, C. Carnegie, H. Ohadi, B. de Nijs, R. Esteban, J. Aizpurua, and J. J. Baumberg, Single-molecule optomechanics in "picocavities", Science **354**, 726 (2016).
[8] K. Y. Yang, D. Y. Oh, S. H. Lee, Q.-F. Yang, X. Yi, B. Shen, H. Wang, and K. Vahala, Bridging ultrahigh-Q devices and photonic circuits, Nat. Photonics **12**, 297 (2018).
[9] T. W. Ebbesen, Hybrid light–matter states in a molecular and material science perspective, Acc. Chem. Res. **49**, 2403 (2016).
[10] X. Zhong, T. Chervy, S. Wang, J. George, A. Thomas, J. A. Hutchison, E. Devaux, C. Genet, and T. W. Ebbesen, Nonradiative energy transfer mediated by hybrid light-matter states, Angew. Chem. **128**, 6310 (2016).
[11] R. Chikkaraddy, B. de Nijs, F. Benz, S. J. Barrow, O. A. Scherman, E. Rosta, A. Demetriadou, P. Fox, O. Hess, and J. J. Baumberg, Single-molecule strong coupling at room temperature in plasmonic nanocavities, Nature (London) **535**, 127 (2016).
[12] B. Gu and S. Mukamel, Manipulating nonadiabatic conical intersection dynamics by optical cavities, Chem. Sci. **11**, 1290 (2020).
[13] M. Kowalewski, K. Bennett, J. R. Rouxel, and S. Mukamel, Monitoring Nonadiabatic Electron-Nuclear Dynamics in Molecules by Attosecond Streaking of Photoelectrons, Phys. Rev. Lett. **117**, 043201 (2016).
[14] K. Bennett, M. Kowalewski, and S. Mukamel, Novel photochemistry of molecular polaritons in optical cavities, Faraday Discuss. **194**, 259 (2016).
[15] C. Schäfer, M. Ruggenthaler, H. Appel, and A. Rubio, Modification of excitation and charge transfer in cavity

quantum-electrodynamical chemistry, Proc. Natl. Acad. Sci. U.S.A. **116**, 4883 (2019).
[16] J. Galego, F. J. Garcia-Vidal, and J. Feist, Cavity-Induced Modifications of Molecular Structure in the Strong-Coupling Regime, Phys. Rev. X **5**, 041022 (2015).
[17] J. Flick, M. Ruggenthaler, H. Appel, and A. Rubio, Atoms and molecules in cavities, from weak to strong coupling in quantum-electrodynamics (QED) chemistry, Proc. Natl. Acad. Sci. U.S.A. **114**, 3026 (2017).
[18] J. Flick, N. Rivera, and P. Narang, Strong light-matter coupling in quantum chemistry and quantum photonics, Nanophotonics **7**, 1479 (2018).
[19] K. E. Dorfman and S. Mukamel, Multidimensional photon correlation spectroscopy of cavity polaritons, Proc. Natl. Acad. Sci. U.S.A. **115**, 1451 (2018).
[20] F. Herrera and F. C. Spano, Absorption and photoluminescence in organic cavity QED, Phys. Rev. A **95**, 053867 (2017).
[21] D. M. Coles, N. Somaschi, P. Michetti, C. Clark, P. G. Lagoudakis, P. G. Savvidis, and D. G. Lidzey, Polariton-mediated energy transfer between organic dyes in a strongly coupled optical microcavity, Nat. Mater. **13**, 712 (2014).
[22] A. F. Kockum, A. Miranowicz, S. De Liberato, S. Savasta, and F. Nori, Ultrastrong coupling between light and matter, Nat. Rev. Phys. **1**, 19 (2019).
[23] P. Vasa and C. Lienau, Strong light–matter interaction in quantum emitter/metal hybrid nanostructures, ACS Photonics **5**, 2 (2018).
[24] M. Hertzog, M. Wang, J. Mony, and K. Börjesson, Strong light–matter interactions: A new direction within chemistry, Chem. Soc. Rev. **48**, 937 (2019).
[25] T. Schwartz, J. A. Hutchison, J. Léonard, C. Genet, S. Haacke, and T. W. Ebbesen, Polariton dynamics under strong light–molecule coupling, Chem. Phys. Chem. **14**, 125 (2013).
[26] F. Herrera and F. C. Spano, Dark Vibronic Polaritons and the Spectroscopy of Organic Microcavities, Phys. Rev. Lett. **118**, 223601 (2017).
[27] L. A. Martínez-Martínez, M. Du, R. F. Ribeiro, S. Kéna-Cohen, and J. Yuen-Zhou, Polariton-assisted singlet fission in acene aggregates, J. Phys. Chem. Lett. **9**, 1951 (2018).
[28] D. Sanvitto and S. Kéna-Cohen, The road towards polaritonic devices, Nat. Mater. **15**, 1061 (2016).
[29] B. Gu and S. Mukamel, Manipulating two-photon-absorption of cavity polaritons by entangled light, J. Phys. Chem. Lett. **11**, 8177 (2020).
[30] A. Mandal and P. Huo, Investigating new reactivities enabled by polariton photochemistry, J. Phys. Chem. Lett. **10**, 5519 (2019).
[31] R. Röhlsberger, J. Evers, and S. Shwartz, Quantum and nonlinear optics with hard x-rays, in *Synchrotron Light Sources and Free-Electron Lasers*, edited by E. J. Jaeschke, S. Khan, J. R. Schneider, and Jerome B. Hastings (Springer International Publishing, Cham, 2020), pp. 1399–1431.
[32] R. Rohlsberger, K. Schlage, B. Sahoo, S. Couet, and R. Ruffer, Collective lamb shift in single-photon superradiance, Science **328**, 1248 (2010).
[33] R. Röhlsberger, H.-C. Wille, K. Schlage, and B. Sahoo, Electromagnetically induced transparency with resonant nuclei in a cavity, Nature (London) **482**, 199 (2012).
[34] J. Haber, J. Gollwitzer, S. Francoual, M. Tolkiehn, J. Strempfer, and R. Röhlsberger, Spectral Control of an X-Ray *L*-Edge Transition via a Thin-Film Cavity, Phys. Rev. Lett. **122**, 123608 (2019).
[35] G. G. Rozenman, K. Akulov, A. Golombek, and T. Schwartz, Long-range transport of organic exciton-polaritons revealed by ultrafast microscopy, ACS Photonics **5**, 105 (2018).
[36] T. Chervy, J. Xu, Y. Duan, C. Wang, L. Mager, M. Frerejean, J. A. W. Münninghoff, P. Tinnemans, J. A. Hutchison, C. Genet, A. E. Rowan, T. Rasing, and T. W. Ebbesen, High-efficiency second-harmonic generation from hybrid light-matter states, Nano Lett. **16**, 7352 (2016).
[37] S. Mukamel, *Principles of Nonlinear Optical Spectroscopy* (Oxford University Press, Oxford, 1995).
[38] B. Xiang, R. F. Ribeiro, A. D. Dunkelberger, J. Wang, Y. Li, B. S. Simpkins, J. C. Owrutsky, J. Yuen-Zhou, and W. Xiong, Two-dimensional infrared spectroscopy of vibrational polaritons, Proc. Natl. Acad. Sci. U.S.A. **115**, 4845 (2018).
[39] C. Pellegrini, A. Marinelli, and S. Reiche, The physics of x-ray free-electron lasers, Rev. Mod. Phys. **88**, 015006 (2016).
[40] S. Mukamel, D. Healion, Y. Zhang, and J. D. Biggs, Multidimensional attosecond resonant x-ray spectroscopy of molecules: Lessons from the optical regime, Annu. Rev. Phys. Chem. **64**, 101 (2013).
[41] S. Tanaka and S. Mukamel, X-ray four-wave mixing in molecules, J. Chem. Phys. **116**, 1877 (2002).
[42] J. D. Biggs, Y. Zhang, D. Healion, and S. Mukamel, Two-dimensional stimulated resonance Raman spectroscopy of molecules with broadband x-ray pulses, J. Chem. Phys. **136**, 174117 (2012).
[43] A. Nenov, F. Segatta, A. Bruner, S. Mukamel, and M. Garavelli, X-ray linear and non-linear spectroscopy of the ESCA molecule, J. Chem. Phys. **151**, 114110 (2019).
[44] See Supplemental Material at http://link.aps.org/supplemental/10.1103/PhysRevLett.126.053201 for details of the electronic structure and spectroscopic computations, which includes Refs. [45–58].
[45] N. Forsberg and P.-A. Malmqvist, Multiconfiguration perturbation theory with imaginary level shift, Chem. Phys. Lett. **274**, 196 (1997).
[46] P.-A. Malmqvist, A. Rendell, and B. O. Roos, The restricted active space self-consistent-field method, implemented with a split graph unitary group approach, J. Phys. Chem. **94**, 5477 (1990).
[47] M. Lundberg and M. G. Delcey, Multiconfigurational Approach to x-ray spectroscopy of transition metal complexes, in *Transition Metals in Coordination Environments*, edited by E. Broclawik, T. Borowski, and M. Radoń (Springer International Publishing, New York, 2019).
[48] K. Andersson, P.-A. Malmqvist, B. O. Roos, A. J. Sadlej, and K. Wolinski, Second-order perturbation theory with a CASSCF reference function, J. Phys. Chem. **94**, 5483 (1990).
[49] V. Sauri, L. Serrano-Andrés, A. R. M. Shahi, L. Gagliardi, S. Vancoillie, and K. Pierloot, Multiconfigurational second-order perturbation theory restricted active space (RASPT2)

method for electronic excited states: A benchmark study, J. Chem. Theory Comput. **7**, 153 (2011).
[50] D. Roca-Sanjuán, F. Aquilante, and R. Lindh, Multiconfiguration second-order perturbation theory approach to strong electron correlation in chemistry and photochemistry, Comput. Mol. Sci. **2**, 585 (2012).
[51] G. Ghigo, B. O. Roos, and P.-A. Malmqvist, A modified definition of the zeroth-order Hamiltonian in multiconfigurational perturbation theory (CASPT2), Chem. Phys. Lett. **396**, 142 (2004).
[52] J. P. Zobel, J. J. Nogueira, and L. González, The IPEA dilemma in CASPT2, Chem. Sci. **8**, 1482 (2017).
[53] T. B. Pedersen, F. Aquilante, and R. Lindh, Density fitting with auxiliary basis sets from Cholesky decompositions, Theor. Chem. Acc. **124**, 1 (2009).
[54] M. Kowalewski, B. P. Fingerhut, K. E. Dorfman, K. Bennett, and S. Mukamel, Simulating coherent multidimensional spectroscopy of nonadiabatic molecular processes: From the infrared to the x-ray regime, Chem. Rev. **117**, 12165 (2017).
[55] B. O. Roos, V. Veryazov, and P.-O. Widmark, Relativistic atomic natural orbital type basis sets for the alkaline and alkaline-earth atoms applied to the ground-state potentials for the corresponding dimers, Theor. Chem. Acc. **111**, 345 (2004).
[56] I. F. Galván *et al.*, OpenMolcas: From source code to insight, J. Chem. Theory Comput. **15**, 5925 (2019).
[57] F. Aquilante *et al.*, Modern quantum chemistry with [Open] Molcas, J. Chem. Phys. **152**, 214117 (2020).
[58] K. E. Dorfman and S. Mukamel, Nonlinear spectroscopy with time- and frequency-gated photon counting: A superoperator diagrammatic approach, Phys. Rev. A **86**, 013810 (2012).
[59] C. A. DelPo, B. Kudisch, K. H. Park, S.-U.-Z. Khan, F. Fassioli, D. Fausti, B. P. Rand, and G. D. Scholes, Polariton transitions in femtosecond transient absorption studies of ultrastrong light–molecule coupling, J. Phys. Chem. Lett. **11**, 2667 (2020).
[60] R. McLaren, S. A. C. Clark, I. Ishii, and A. P. Hitchcock, Absolute oscillator strengths from *K*-shell electron-energy-loss spectra of the fluoroethenes and 1,3-perfluorobutadiene, Phys. Rev. A **36**, 1683 (1987).
[61] S. Schütz, J. Schachenmayer, D. Hagenmüller, G. K. Brennen, T. Volz, V. Sandoghdar, T. W. Ebbesen, C. Genes, and G. Pupillo, Ensemble-Induced Strong Light-Matter Coupling of a Single Quantum Emitter, Phys. Rev. Lett. **124**, 113602 (2020).
[62] A. Muthukrishnan, G. S. Agarwal, and M. O. Scully, Inducing Disallowed Two-Atom Transitions with Temporally Entangled Photons, Phys. Rev. Lett. **93**, 093002 (2004).
[63] M. Richter and S. Mukamel, Collective two-particle resonances induced by photon entanglement, Phys. Rev. A **83**, 063805 (2011).
[64] M. Richter and S. Mukamel, Ultrafast double-quantum-coherence spectroscopy of excitons with entangled photons, Phys. Rev. A **82**, 013820 (2010).
[65] I. V. Schweigert and S. Mukamel, Double-quantum-coherence attosecond x-ray spectroscopy of spatially separated, spectrally overlapping core-electron transitions, Phys. Rev. A **78**, 052509 (2008).
[66] J. Kim, S. Mukamel, and G. D. Scholes, Two-dimensional electronic double-quantum coherence spectroscopy, Acc. Chem. Res. **42**, 1375 (2009).
[67] X. Dai, M. Richter, H. Li, A. D. Bristow, C. Falvo, S. Mukamel, and S. T. Cundiff, Two-Dimensional Double-Quantum Spectra Reveal Collective Resonances in an Atomic Vapor, Phys. Rev. Lett. **108**, 193201 (2012).
[68] D. Abramavicius, A. Nemeth, F. Milota, J. Sperling, S. Mukamel, and H. F. Kauffmann, Weak Exciton Scattering in Molecular Nanotubes Revealed by Double-Quantum Two-Dimensional Electronic Spectroscopy, Phys. Rev. Lett. **108**, 067401 (2012).
[69] Here, $\Rightarrow$ indicates a double excitation.
[70] A. Nenov, I. Rivalta, S. Mukamel, and M. Garavelli, Bidimensional electronic spectroscopy on indole in gas phase and in water from first principles, Comput. Theor. Chem., **1040–1041**, 295 (2014).
[71] Here, the brackets indicate that the core-excitation occurs in the presence of a core-excited carbon.
[72] J. A. Hutchison, T. Schwartz, C. Genet, E. Devaux, and T. W. Ebbesen, Modifying chemical landscapes by coupling to vacuum fields, Angew. Chem., Int. Ed. Engl. **51**, 1592 (2012).